RSC Advances

ROYAL SOCIETY OF CHEMISTRY

www.rsc.org/advances

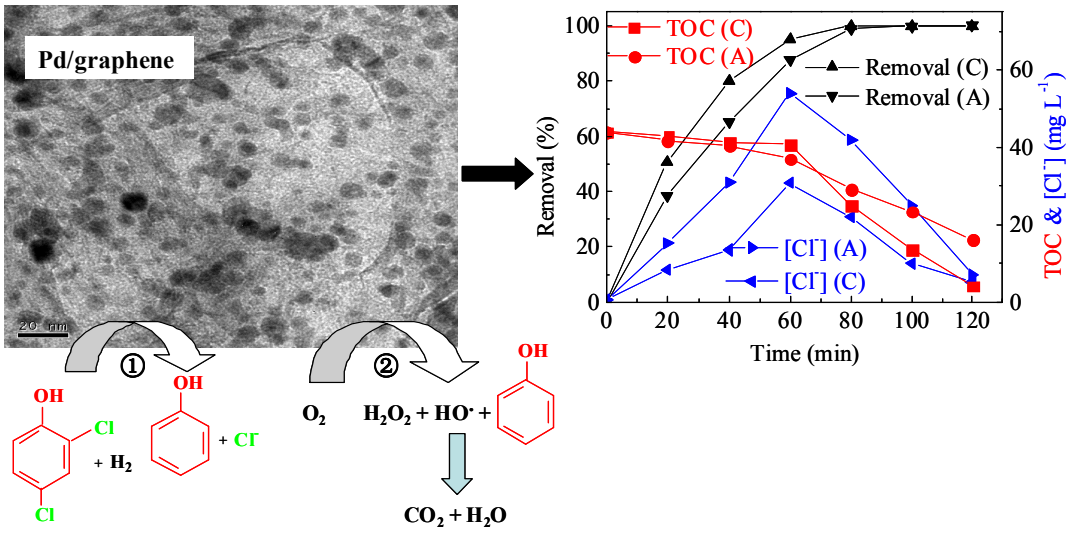

The Pd/graphene gas-diffusion cathode exhibits high electrocatalytic dechlorination activity.

Electrocatalytic degradation of 2,4-dichlorophenol on a Pd/graphene gas-diffusion electrode

Qin Shi[a], Hui Wang[a,*], Shaolei Liu[a] and Zhaoyong Bian[b,**]

[a] *College of Environmental Science and Engineering, Beijing Forestry University, Beijing 100083, PR China*

[b] *College of Water Sciences, Beijing Normal University, Beijing 100875, PR China*

Abstract

The palladium-modified graphene gas-diffusion cathodes were achieved using prepared Pd/grapheme catalysts whose were well-characterized by using cyclic voltammetry, scanning electron microscopy, transmission electron microscopy, X-ray diffraction, Raman spectroscopy, Fourier transform infrared spectrometry. The Pd particles with an average size of 5.4 nm had an amorphous structure with dispersing highly in the graphene. A diaphragm electrolysis system sequentially fed with H_2 and air over the gas-diffusion cathodes was constructed and applied for the 2,4-dichlorophenol (2,4-DCP) degradation. Reductive dechlorination of 2,4-DCP was performed when the Pd/graphene gas-diffusion cathodes were feeding with H_2, while acceleration of two-electron reduction of O_2 to H_2O_2 proceeded with air. Therefore, the degree of dechlorination for 2,4-DCP reached approximately 96.4% after 60 min, while the removal efficiency and the average removal efficiency of 2,4-DCP in terms of total organic carbon (TOC) after 120 min reached approximately 100% and 90.5%, respectively. Furthermore, analyzing the electrolysis intermediates

* Corresponding author. Tel.: +86 10 62336615; fax: +86 10 62336596
E-mail address: wanghui@bjfu.edu.cn
** Corresponding author. Tel.: +86 10 58802736; fax: +86 10 58802739
E-mail address: bian@bnu.edu.cn

used of HPLC and IC, a reaction pathway was proposed for the degradation of 2,4-DCP.

Keywords: Electrocatalytic technology; Gas-diffusion cathode; Pd/graphene catalyst; Chlorophenol; Priority pollutant.

1. Introduction

Chlorophenol compounds are important reagents and reactants for the industrial products such as paper, medicines, and wood preservatives.[1-5] The wastewater generated during production and product utilization of chlorophenol compounds will eventually be released into the environment as a serious pollutant.[6-9] 2,4-DCP is resistant to degradation and exists in wastewater form pesticide, fuel and plasticizer production and has been listed as a priority control pollutant in both the US and China. However, these compounds are difficult to degrade, making them long-term residents to water and soil environments, and incorporating into the bodies of humans and animals. Hence, methods developed to remove these materials and studies concerning organic matter have become a popular research pursuit in recent years.

Electrochemical methods could be used to degrade chlorophenol compounds because it requires simple equipments and is easily operated.[10,11] However, the catalytic electrode exhibits good degradation effects for low chlorophenol concentrations and requires long reaction times to attain high chlorophenol removal rates. In addition, the direct electrochemical oxidation and reduction of chlorophenols may produce large amounts of toxic chlorided intermediate products. Therefore, the electrolytic solutions

shows higher toxicity compared with their parent solutions.

In the research toward electrochemical chlorophenol degradation, palladiumm attracts much attention due to its good catalytic performance on the hydrodechlorination.[12-17] To maximize the activity of the Pd while minimizing its content, highly reactive Pd nanostructures must be loaded on the surface of inexpensive nanomaterial with high surface areas and good electrical conductivity; this type of system maximizes the availability of the nanoscale electrocatalytic surface area for electron transfer while facilitating better mass transport of reactants to the electrocatalyst. Although activated carbon (AC)[18-22] and carbon nanotubes (CNTs)[23] are good carriers, they do not display particularly good hydrogenation/dechlorination performance.

Graphene is one kind of carbon materials composed of sp^2 bonded carbon atoms arranged in single-layered hexagonal lattices.[24-27] As a new type of nanoscale two dimensional carbon materials,[28] it demonstrates good electric conducity, constant chemical stability, and numerous surface folds with high surface area.[29,30] Compared to AC and CNTs, graphene is an optimal material with reinforcing nanocomposites due to its outstanding properties and abundant precursors.[31] Several methods have been developed to produce graphene sheets.[32-35] Most of these methods require high temperatures and long processing times. Chemically reducing exfoliated graphite oxide (GO) with reagents, such as formaldehyde,[36,37] provides a promising approach toward to product chemically converted graphene (CCG) sheets efficiently in large scale. This

paper reports solution-based methods for preparing Pd-modified graphene nanosheets. Both processes of GO reduction and in-situ Pd nanoparticle deposition were accomplished in a one-step process.

This paper had investigated the catalytic oxidation and reduction of 2,4-dichlorophenol (2,4-DCP) on a Pd/graphene gas-diffusion electrode. First, the prepared Pd/graphene catalyst used in the gas-diffusion electrode was characterized by Raman spectroscopy, Fourier transform infrared spectrometry (FTIR), X-ray photoelectron spectroscopy (XPS), X-ray diffraction (XRD), transmission electron microscopy (TEM), scanning electron microscopy (SEM), and cyclic voltammetry (CV). Subsequently, 2,4-DCP was degraded in a diaphragm electrolysis system containing a $Ti/IrO_2/RuO_2$ anode, a Pd/graphene gas-diffusion cathode and a synthesized organic membrane. Under the reductive dechlorination removing the chlorine atoms of 2,4-DCP from the aromatic structure, non-chlorinated intermediates was forming in the cathodic compartment. And then, in the anodic and cathodic compartments, oxidization and degradation of these intermediates continued. Finally, we identified the major intermediates of the 2,4-DCP degradation using chromatography technologies and proposed the reaction pathway.

2. Experimental section

2.1. Preparation of Pd/graphene catalyst

Preparing the Pd/graphene catalyst involves three key steps: (i) oxidizing the starting graphite to form pre-oxidized graphite, (ii) oxidizing the pre-oxidized graphite

to obtain GO, and (iii) the one-step formaldehyde reduction and dispersion of the Pd^{2+}-GO that produces the Pd/graphene catalyst.

GO was prepared from natural graphite flakes (99.99%, 325 mesh, Qingdao Zhongtian Company, Qingdao, China) using a protocol based on a modification of Hummers method.[38,39] The graphite powder (2 g) was added to an 80 °C solution of concentrated H_2SO_4 (30 mL), $K_2S_2O_8$ (2 g), and P_2O_5 (2 g). The mixture was stirred at 80 °C for 6 h before being allowed to cool to 25 °C. The mixture was then carefully diluted with distilled water, filtered, and washed on the filter until the rinses attain a neutral pH. The product was dried in air at ambient temperatures overnight, obtaining the pre-oxidized graphite.

This pre-oxidized graphite (1 g) was placed in cold (0 ^oC) concentrated H_2SO_4 (25 mL). $KMnO_4$ (6 g) was added gradually with stirring and cooling such that the temperature remained below 20 °C; the mixture was subsequently stirred for 2 h. Afterward, the solution was heated to 35 °C for 30 min before distilled water (50 mL) was added. After 15 min, the reaction was terminated by adding a massive excess of distilled water (250 mL) and 30% H_2O_2 solution (4.25 mL), changing the color of the mixture to bright yellow. The mixture was filtered and washed with a 1:10 HCl solution (500 mL) to remove any metal ions. The product was filtered, washed with water, and centrifuged until the supernatant pH = 5. Finally, the suspension was dried in a vacuum oven at 60 ºC for 48 h to obtain GO.

A formaldehyde reduction method was used to prepare Pd/graphene catalysts.

Dissolved $PdCl_2$ in the concentrated hydrochloric acid, subsequently mixed with 15 mL of deionized water. A GO solution was added dropwise into the $PdCl_2$ solution with vigorous stirring at 80 °C. The mixture was maintained at 80 °C for another 2 h and cooled to 40 °C. Then 36% formaldehyde solution was added into the prepared solution with vigorous stirring. The solution was heated to 80°C and the pH of the solution was adjusted to 8-9 using 30% NaOH solution. Finally, Pd/graphene catalysts loaded with 1.0 wt.% Pd were filtered and washed with pure water for six times.

2.2. Procedures

The preparation of Pd/graphene gas-diffusion cathodes and a schematic diagram of the experimental were in accordance with a previously reported procedure.[40] The electrolytic action was performed in a 100-mL diaphragm electrolysis device contained a gas-diffusion cathode (16 cm^2) and a $Ti/IrO_2/RuO_2$ anode (16 cm^2). A direct-current laboratory power supplied with a monitor for current-voltage provided the electricity. The conditions of the experiments were the following: the original concentration of 2,4-DCP was 100 mg L^{-1}; the supporting electrolyte (Na_2SO_4) concentration was 0.03 mol L^{-1}; the pH value of original solution was 7.0; and the current density was 50 mA cm^{-2}. The gas compartment was fed with H_2 at 25 mL s^{-1} over a 0-60 min, followed by air.

2.3. Analytical methods

The Raman spectra were collected on an inVia-Reflex Raman spectroscope equipped with a 514.5 nm laser source (British Renishaw). A FTIR was used to analyze

the changes in functional groups on the catalyst. The sample powder was ground with KBr and pressed to prepare a pellet. A Nicolet 2550 spectrometer was used to study the formaldehyde reduction of GO. The spectra were acquired in an optical range of 500-4000 cm^{-1} by averaging 8 scans with a 4 cm^{-1} resolution. The Pd/graphene catalyst was characterized using XRD with an X' Pert PRO MPD X-ray power diffractometer using Cu Kα radiation with a Ni filter. An S-4800 SEM was used to study the surface morphology. The morphological characteristic and size distributing characteristic of Pd particle were determined by TEM (JEM-2010F TEM microscope) under the operating conditions of 200 kV.

The cyclic voltammetry characteristics were studied by using a potentiostat/galvanostat (EG&G Model 273A) with a standard three-electrode system. The three-electrode system was consist of an Ag/AgCl electrode as the reference electrode; a Pt wire as the counter electrode, and the Pd/graphene catalyst-modified electrode as the working electrode.

The high performance liquid chromatography (HPLC, Shimadzu, Japan) was used to determine 2,4-DCP and its stable electrolyzed products through the means of comparison of the retention times to their the standard compounds. The samples (20 μL) were passed through 0.45 μm PTFE filters before given injection into the HPLC. The Znertisl ODS-SP C18 column (250 mm × 4.6 mm, 5 μm) would carry out the separation whose flow rate was at 1.0 mL min^{-1} and temperature was 30°C. The determination of aromatic compounds was performed using HPLC with setting UV-detector at 280 nm

and containing mobile phase methanol/water (v/v) 80/20. Similarly, the determination of carboxylic acids was also performed using HPLC with setting UV-detector at 210 nm and containing mobile phase methanol/KH_2PO_4 (v/v) 25/75 (kept the pH at 2.1 by adjusting with H_3PO_4).

Ion chromatography (ICS-3000, Dionex, America) was used to assess the content of the small carboxylic acids and the chloride ionic concentration in the electrolyte with the comparison of the retention times to their standard compounds. The samples were passed through 0.45 μm PTFE filters and given injection into the IC. The AS-11 column would carry out the separation with a flow rate was at 1.2 mL min^{-1} and temperature was 30°C. The mobile phase consisted of 5% (vol.) NaOH (5 mmol L^{-1}) and 95% (vol.) deionized water during the 0-6 min period; the volume of NaOH was increased to 12% during the 6-41 min period, reduced to 5% during the 41-42 min period and remained at 5% during the 42-50 min period.

Detection of total organic carbon (TOC) was performed by using Elementar High TOC analyzer.

3. Results and discussion

*3.1. Characterization of Pd/*graphene *catalyst*

A typical Raman spectrum of carbonaceous materials exhibited two characteristic bonds as follow: the G band at approximately 1580 cm^{-1} which attributed to sp^2 bonded carbon atoms in a hexagonal lattice; the D band at approximately 1350 cm^{-1} related to the vibrations of sp^3 carbon atoms due to defects and disorder.[41] As shown in Fig. 1, the

Raman spectrum of the pristine graphite displayed a weak D band at 1357 cm^{-1}, a strong G band at 1578 cm^{-1}, and a middle 2D band at 2716 cm^{-1}. The peak intensity ratio of the D-band and G-band was a quality measurement of graphitic structures because this ratio approached to zero for highly ordered, pyrolysis graphite.[42] The Raman spectrum of the natural graphite showed a low D/G intensity ratio (0.04). The broadened G band peak and the enlarged D band peak with a high D/G intensity ratio (1.06) could be observed for GO samples as a result of the oxidation generated a high level of disorder in the graphene nanosheets. However, the D/G ratio was 0.95 for the Pd/graphene catalyst. It indicated that new, more numerous, smaller graphitic domains are produced when Pd/graphene formed.[41] In addition, there was a significant change in 2D band of the Pd/graphene compared to that of bulk graphite. The weak and broadened 2D peak revealed that the Pd/graphene possessed some defects caused by the fast reduction process.[43] These structural deficiencies might enhance the catalytic activity of the Pd/graphene catalyst.

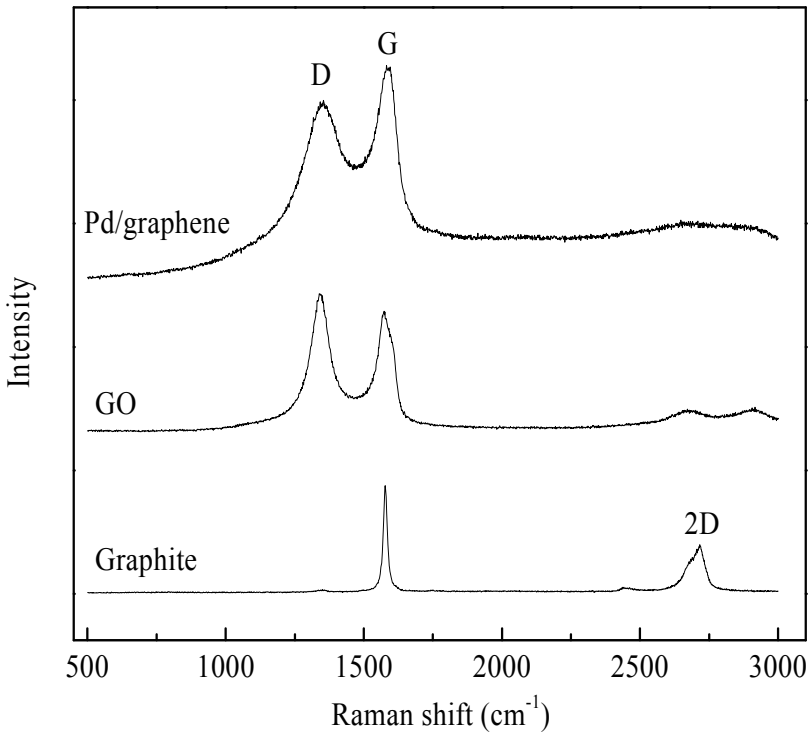

Fig. 1. Raman spectra of the graphite, GO, and Pd/graphene catalysts.

Fig. 2 shows the FTIR spectra of GO, the graphite, and Pd/graphene catalysts. The results indicated that various oxygen-containing functional groups have been removed from the graphite oxide plane *via* formaldehyde reduction. The GO spectrum contained resonances for O-H (broad coupling ν(O-H)) at 3200 cm^{-1} (carboxylic acid), O-H (ν(carboxyl)) at 1363 cm^{-1}, and for the O-H stretching mode of intercalated water at 3392 cm^{-1},[44] as well as C=O for the carboxylic acid and carbonyl moieties (ν(carbonyl)) at 1734 cm^{-1}, C-O (ν(epoxy or alkoxy)) at 1055 cm^{-1}, and for C=C at 1618 cm^{-1} from the skeletal vibrations of unoxidized graphitic domains or contribution from the stretching

deformation vibration of intercalated water. After the chemical reduction of the Pd/grapheme, the C=O vibration band, the broad O-H (1363 cm^{-1}), and the C-O stretching bands became weakly (carboxyl groups are greatly reduced, similar to original graphite) while one peak still keep at 1618 cm^{-1}, similar to original graphite. Therefore, highly regular pure graphene could be generated via the formaldehyde reduction.

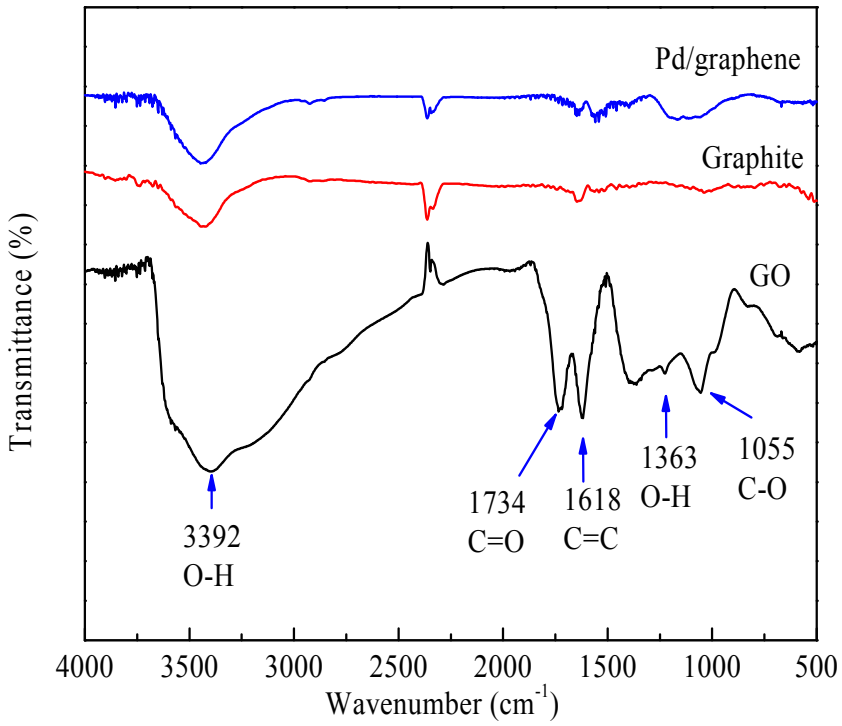

Fig. 2. FRIT patterns for the graphite, GO, and Pd/graphene catalysts.

The XRD patterns of the prepared materials are shown in Fig. 3. The initial graphite powder displayed a typical sharp diffraction peak at 2θ=26.5° with a

corresponding calculated 3.4 Å *d*-spacing. The GO sample exhibited no diffraction peaks attributed to graphite, with a new broad peak at 2θ=12.1° with a calculated 7.3 Å *d*-spacing. The interlayer distance significantly expanded after the oxidation which attributed to the formation of hydroxyl, epoxy, and carboxyl groups.[45,46] However, the peak at 2θ=12.1° disappeared and a new obvious diffraction peak at 2θ=39.7° contributed to the Pd planes (111) appeared in the XRD pattern of the Pd/graphene. It indicated that the GO sheets had been reduced completely and Pd particles were loaded on the graphene supporting with a 2.3 Å d-spacing. When graphene was formed, the d-spacing significantly decreased due to the removal of oxygen-functional groups. The XRD peaks exhibited features of face-centered-cubic crystalline Pd, corresponding to the (111), (220), and (311) planes (2θ=39.7^{o}, 67.6^{o}, and 80.7^{o}), respectively. Moreover, nanoparticle size of the metal palladiums in Pd/graphene was approximately 5.4 nm which was calculated using the Pd (111) diffraction line with the Scherrer equation.[47] Hence, the palladium nanoparticles conformably distributed on the graphene supporting.

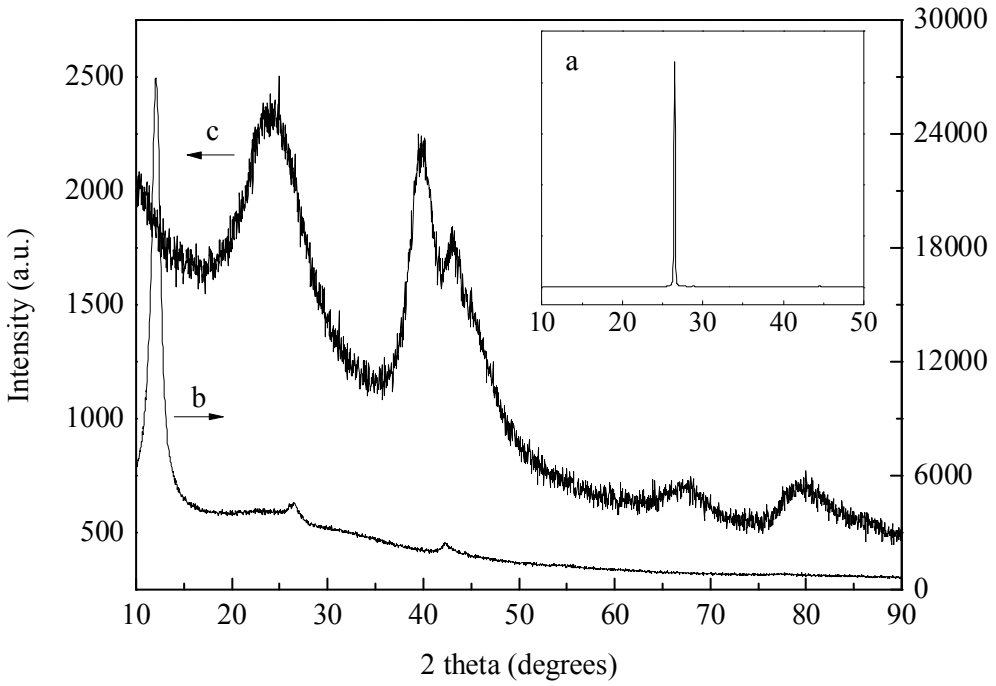

Fig. 3. X-ray diffraction patterns of the graphite (a), GO (b), and Pd/graphene catalysts (c).

The state of catalytic metal particles and surface properties of the supporting materials are key factors influencing metal loaded catalyst performance. Fig. 4 shows the SEM patterns of the graphite, GO and Pd/graphene catalysts. Graphite consisted of large stacks (shown in Fig. 4a), while GO was exfoliated to form thin wrinkled flakes (in Fig. 4b). As shown in the SEM pattern of the Pd/graphene catalysts (Fig. 4c), the Pd nanoparticles appeared as discrete bright dots homogeneously distributed on the folded silk like graphene surfaces. During the reduction process, although Pd was primarily loaded in the folds with agglomerated Pd at the top of folds, most Pd particles were

small and spread at the edge of folds.

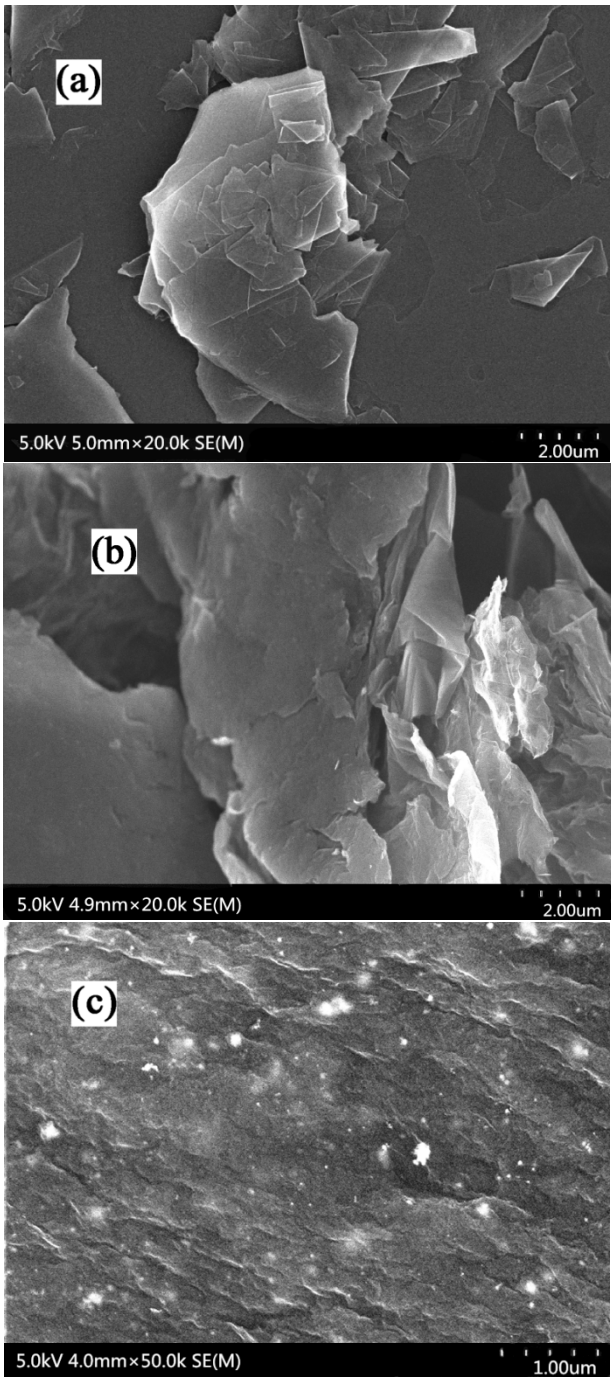

Fig. 4. SEM images of the graphite (a), GO (b), and Pd/graphene catalysts (c).

The morphology and structure of the Pd/graphene catalysts was characterized by TEM as shown in Fig. 5. In the Pd/graphene catalyst (Pd particles average particle size,

6.1±0.3 nm), the observation was that the palladium nanoparticles were in uniform size and well dispersing. The average size of the Pd nanoparticles obtained from TEM images was consistent with the XRD results. The epoxy and hydroxyl groups of GO in the Pd/graphene catalysts contributed to the small and well dispersion of Pd nanoparticles on the graphene. These surface groups fixed the Pd precursor and prevented Pd aggregation which is in favor of the Pd nanoparticle dispersion on GO.[48]

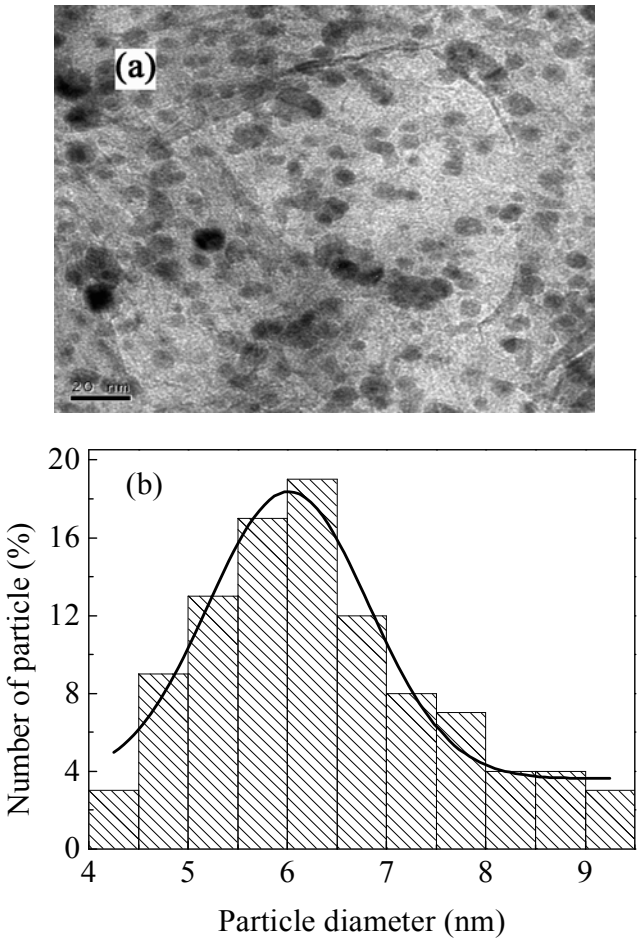

Fig. 5. TEM images (a) and the particle size statistics (b) of Pd/graphene catalysts.

Fig. 6 shows the cyclic voltammogram for the Pd/graphene catalyst electrode surface under different gases atmosphere in a Na_2SO_4 electrolyte (0.03 mol/L, keep the

pH at 12.8 by adjusting with a NaOH solution). A strong reductive peak appeared at -0.50 V in an O_2 saturated alkaline solution due to the two-electron reduction of O_2 to peroxide anions (HO_2^-). This reductive peak disappeared when O_2 was replaced by N_2 under the same conditions. In addition, the reduction peak intensity enhanced as potential shifted to negative with increased sweep rates (v). The correlation coefficient of the peak current intensity with the sweep rate was 0.803, indicating an irreversible homogeneous chemical reaction occurred (shown in Fig. 7). Based on the calculations, the reduction was diffusion-controlled based on the linear dependence of the peak current i_p on $v^{1/2}$ (R^2=0.988) (inset in Fig. 7).

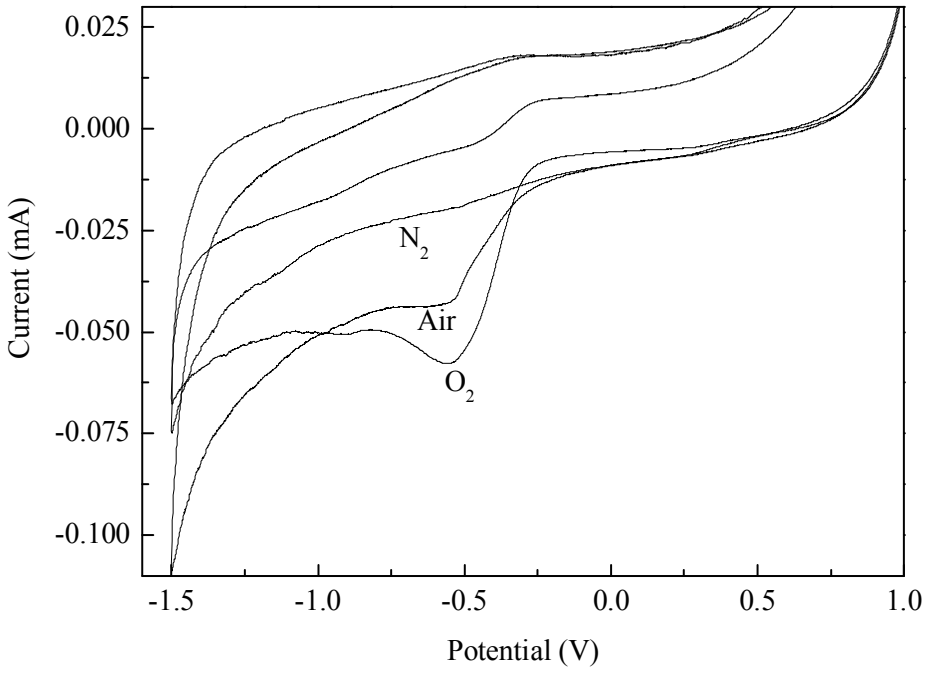

Fig. 6. CV curves for the Pd/graphene catalyst electrode in 0.03 mol L^{-1} Na_2SO_4 solution (pH=12.8, fed with N_2, air, and O_2) at 100 mV s^{-1}.

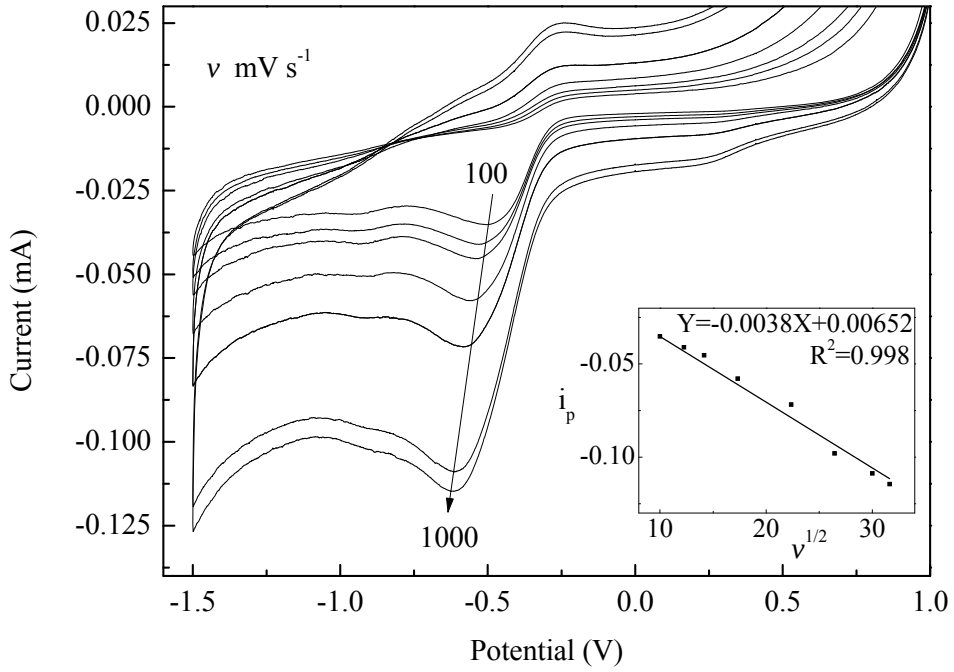

Fig. 7. Cyclic voltammograms of the Pd/graphene catalyst electrode in 0.03 mol L^{-1} Na_2SO_4 solution (pH=12.8, fed with O_2) at 100-1000 mV s^{-1}.

3.2. Removal and dechlorination of 2,4-DCP

Fig. 8 shows the removal percentage for 2,4-DCP and variations in the TOC within the anodic and cathodic chambers with the electrolysis times when feeding with hydrogen and air in the Pd/graphene gas-diffusion electrode system.

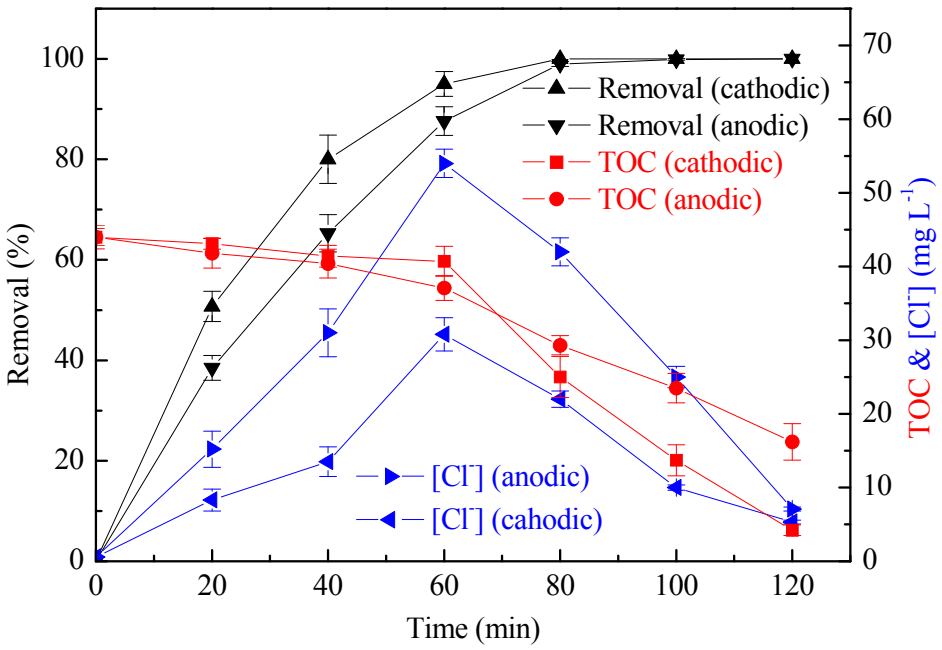

Fig. 8. Removal of 2,4-DCP while varying the TOC & [Cl^-] in the cathodic and anodic chambers and the electrolysis time under H_2 and air feed using the Pd/graphene gas-diffusion electrode system.

The removal percentage of 2,4-DCP in the cathodic chamber was increasing at the first 60 min of working time while using the Pd/graphene gas diffusion electrode fed with H_2. Pd was an excellent catalyst for hydrogenolysis, and the existence of Pd in the graphene nanoparticles was effective for accelerating dechlorination. Consequently the degradation percentage of 2,4-DCP could be improved to approximately 100% after 80 min. But during first 60 min, the TOC degradation percentage in the cathodic chamber improved slightly. After 60 min, with feeding air instead of H_2, the TOC degradation percentage in the cathodic chamber enhanced significantly to reach 90.5% at 120 min

(Fig. 8). During the first 60 min, it was suggested that there was no further oxidation between non-chloride intermediates to product CO_2 and H_2O in the cathodic chamber; this chamber also did not form H_2O_2 through the electrochemical reduction of dissolved oxygen with H_2 feeding. After 60 min, the two-electron reduction of O_2 was catalyzed to form H_2O_2 and HO_2^- with the help of the Pd/graphene gas-diffusion electrode. And these species were transformed into $HO\cdot$ and O_2^- in air.[40] Hence, the Pd/graphene catalyst of Pd/graphene gas-diffusion electrode system could accelerate the two-electron reduction of O_2 to H_2O_2 with feeding air, was in accord with cyclic voltammetry data (Fig. 6).

The change trends of 2,4-DCP degradation percentage in the anodic chamber and those in the cathodic chamber exhibited similarity in the Pd/graphene gas-diffusion electrode systems (shown in Fig. 8). But the degradation percentages of TOC and 2,4-DCP in the anodic chamber were not higher than that in the cathodic chamber. It still had difficulty in achieving total mineralization during the anodic oxidation due to the small amount of $MO_x(OH\cdot)$ or MO_{x+1} came from the surface of the anode, though the 2,4-DCP removal was attributed to their oxidizing action.[49-51] But the oxidation ability of H_2O_2, $HO\cdot$ and $O_2^{-}\cdot$, which were produced in the electrolyte by the O_2 electro-reduction on the Pd/graphene gas-diffusion cathode, still kept strong and could degrade organic molecules to be smaller, even H_2O and CO_2. Consequently, the 2,4-DCP was mineralized in the cathodic chamber better than in the anodic chamber.

2,4-DCP is toxic and non-biodegradable due to its chlorine functional groups. To

analyze the removal of the chlorine functional groups from 2,4-DCP during the degradation process, the chloride ion concentration in the reaction solution was measured with an ion chromatograph. Fig. 8 displays the variations in the chloride ion concentrations in the anodic and cathodic chambers with the electrolysis time while feeding hydrogen gas and air into the Pd/graphene gas-diffusion electrode system. The change trends of chloride ion concentration in the anodic and cathodic chambers have similarity in the Pd/graphene gas-diffusion electrode systems. As observed in Fig. 8, as the reaction time increased, the chloride ion concentration in the aqueous solution gradually increased, reaching 30.8 mg L^{-1} and 54.0 mg L^{-1} in the cathodic and anodic chambers at 60 min, respectively. And the degree of dechlorination in the 2,4-DCP reached 96.4% at 60 min, demonstrating that the chlorine atoms on the aromatic ring mainly released to form chloride ions. However, chloride ions concentration in anodic chamber was higher than that in cathodic chamber. Because the chloride ions of cathodic chamber diffused into anodic chamber through the terylene membrane as a result of electrostatic repulsion form cathode which carry negative charge. Therefore, the chloride ion concentrations in the anodic chamber were high. After increased electrolysis times, the chloride ion concentration decreased in both chambers. Cl_2 gas released on the anode attribute to the oxidation which turned chloride ion into Cl_2 gas, and it also was reported during BDD anodes were using to electrolyze chloroprene.[52] Hydrogen gas was fed into the Pd/graphene gas-diffusion electrode system at the first 60 min. There was hydrodechlorination reactions of 2,4-DCP mainly but little

mineralization. The C-Cl bond was broken and -Cl was replaced by active hydrogen species to generate Cl^-. So TOC removal is slow at the first 60 min and the Cl^- is first increased. After 60 min, with feeding air instead of feeding hydrogen gas, Pd/graphene gas-diffusion electrode catalyzed the two electron reduction of O_2 to H_2O_2 and HO_2^-, and then H_2O_2 and HO_2^- may be converted to HO· and O_2^{-}·. TOC removal was fast with mineralization and Cl^- was immediately driven away from the reaction system as Cl_2. So the concentration of Cl^- decreased. In this experiments, HOCl could not be determined, the results obtained were different to published value.[53,54] Actually, in the electrolysis processes, HOCl will react and oxide organic compounds to form more toxic intermediates. Hence, in the design of an electrolysis system for wastewater treatment, HOCl should be avoided as much as possible. In the cathodic chamber, the zero-valence Pd could promote a hydrogenolysis reaction to replace the chlorine atom in a chlorinated organic compound with a hydrogen atom. In the anodic chamber, the C-Cl bond on the benzene ring was broken by HO· due to its incredibly strong oxidation capacity during electrocatalytic processes. Subsequently, the chlorine substituent became a free chloride ion. Accordingly, the toxicity of 2,4-DCP was reduced, improving its biodegradability.

3.3. Identification of intermediates and their evolution

According the classical 2,4-DCP reduction and oxidation scheme proposed in previous reports,[55,56] an exhaustive analysis of intermediates in the Pd/graphene gas-diffusion electrode system was performed using HPLC and IC. The TOC has also

been used to evaluate the total organic materials in the reaction samples. A comparison of the measured TOC values (by TOC analyzer) and the carbon bound values calculated from the concentrations of the 2,4-DCP and the intermediates ($C_{DCP+Int}$) is presented in Figs. 9a and 10a. As expected, the $C_{DCP+Int}$ values are slightly lower than the measured TOC values; however, the discrepancy is only 6%, indicating that the main reaction intermediates are detected. Figs. 9 and 10 display the changes in the concentration of every aromatic intermediate and carboxylic acid present during the 2,4-DCP degradation over the Pd/graphene gas-diffusion electrode system.

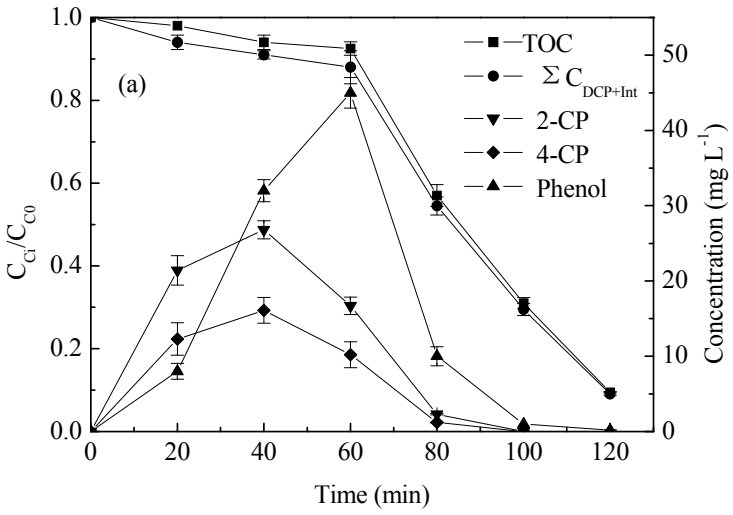

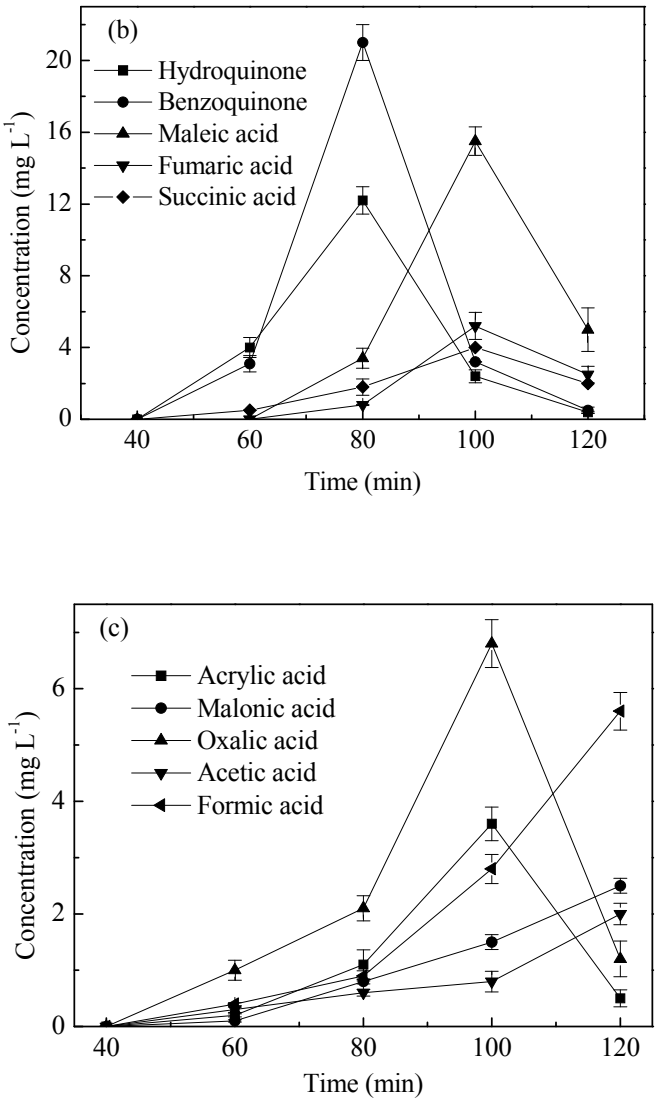

Fig. 9. Changes in the concentration of 2,4-DCP and main intermediates in the cathodic chamber during the degradation of 2,4-DCP using the Pd/graphene gas-diffusion electrode system.

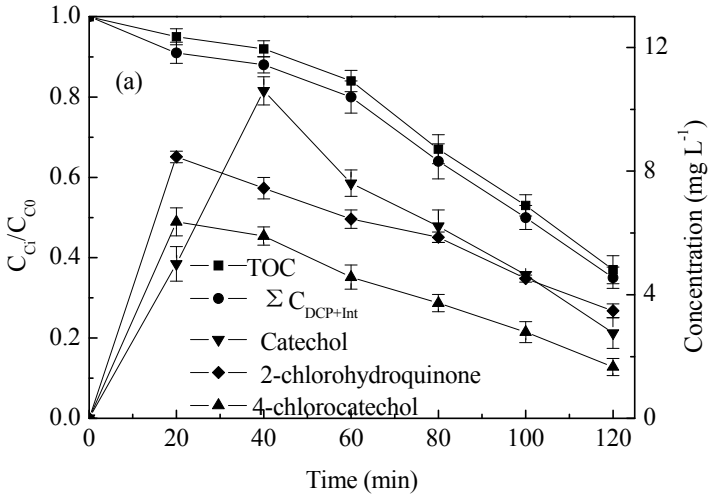

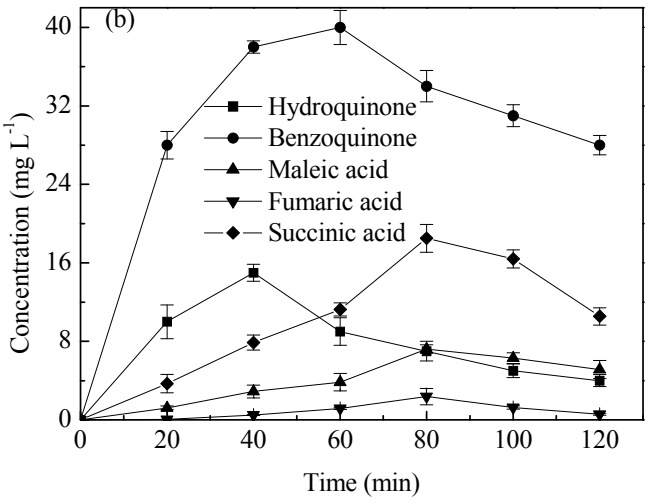

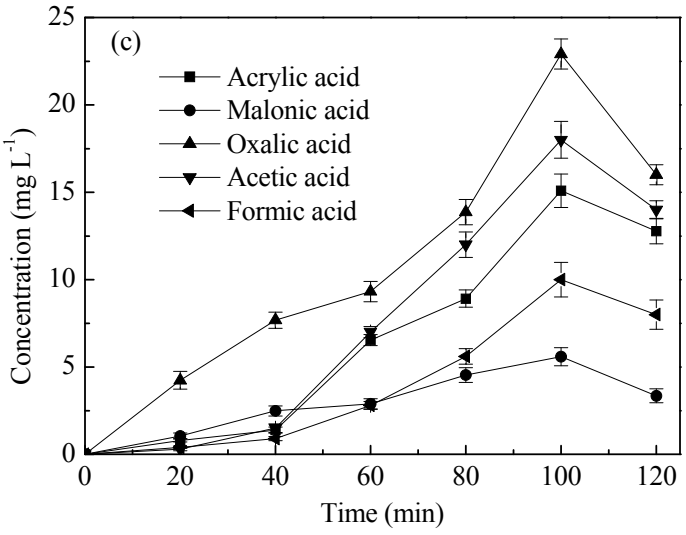

Fig. 10. Changes in the concentration of 2,4-DCP and main intermediates in the anodic chamber during the degradation of 2,4-DCP using the Pd/graphene gas-diffusion electrode system.

In the cathodic chamber, 2,4-DCP was initially reduced to form 2-CP and 4-CP before being converted to phenol (0-60 min) under hydrogen gas in the Pd/graphene gas-diffusion electrode system. The generation and further catalytic reduction of 2-CP and 4-CP are presented in Fig. 9a. The concentration 2-CP and 4-CP was initially increased and followed by a slow decrease. Although during further catalytic reduction processes the 2-CP was reduced to phenol more easily than 4-CP, the concentration of 4-CP was lower than that of 2-CP, meaning that the reactivity of Cl at the 4-position in 2,4-DCP is higher than that of the Cl in the 2-position. The peak concentrations of 2-CP and 4-CP were 26.8 mg L^{-1} and 16.1 mg L^{-1} at 40 min. The phenol content increased to reach a maximum value of 45.0 mg L^{-1} at 60 min, while the concentration of 2,4-DCP decreased rapidly. After 100 min, the concentration of phenol was low, and 2,4-DCP, 2-CP and 4-CP could not be detected. As presented in Fig. 9b and 9c, the concentration of aromatic intermediates (hydroquinone and benzoquinone) initially increased slowly 40 min before peaking at approximately 80 min and decreasing to zero within 120 min. Maleic, fumaric, and succinic, acrylic and oxalic acid acids were gradually formed, achieving their peak values at approximately 100 min before decreasing. Malonic, acetic and formic acids formed gradually and persisted in solution after 120 min of

reaction.

As shown in Fig. 10, the HPLC and IC analyses of the anodic chamber revealed the maximum concentrations of the main intermediate products at different times, as well as their subsequent decreases. After 120 min, most of the intermediate products were transformed into CO_2 and H_2O. Analyzing the concentration histories of these intermediates relative to time reveals the trends typical of a consecutive-parallel reaction pathway. After considering the experimental results analyzed above, a reaction pathway for 2,4-DCP degradation was proposed in Fig. 11.

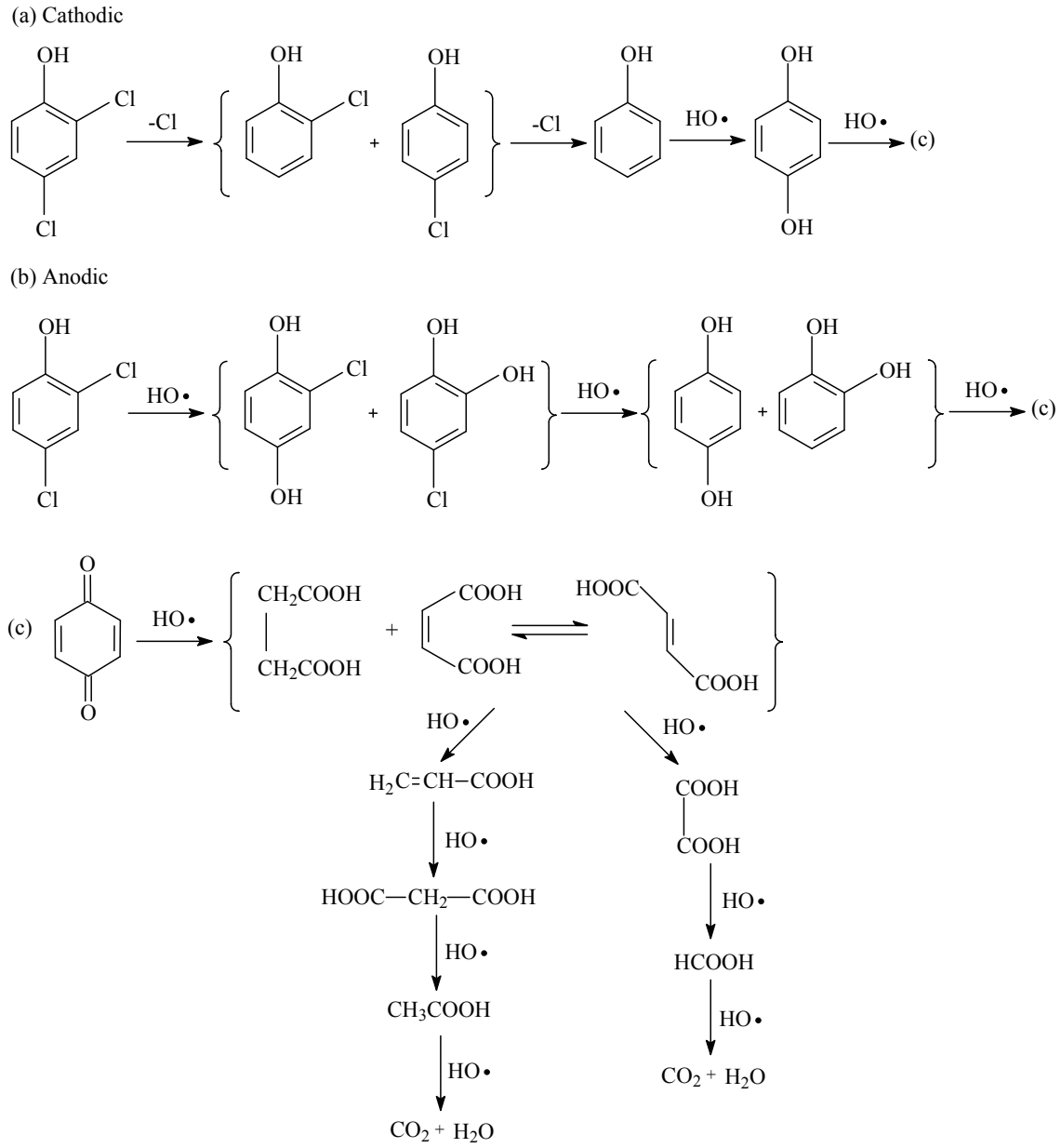

Fig. 11. Degradation pathway for 2,4-DCP for the Pd/graphene gas-diffusion electrode system.

In the cathodic chamber, there were two possible degradation pathways for 2,4-DCP in aqueous solutions involving reductive dechlorination and oxidative hydroxylation reactions, represented in Scheme (a). Briefly, one -Cl was replaced by an active

hydrogen species to generate 2-CP or 4-CP. Subsequently, both 2-CP and 4-CP were dechlorinated to form phenol which was the main intermediate under reductive conditions. Consequently, the phenol underwent a hydroxylation reaction to generate hydroquinone. Further reactions yielded the corresponding benzoquinone under oxidative conditions. For the anodic chamber and according to the hydroxyl radical-based oxidation mechanism accepted by many researchers,[49,57] a detailed analysis of the intermediate products revealed that the oxidation initiated with the aromatic hydroxylation via hydroxyl radicals generated on the $Ti/IrO_2/RuO_2$ anode surface (Fig. 11b). The hydroxyl radicals added to 2,4-DCP, generating 4-chlorohydroquinone and 2-chlorocatechol. These intermediates formed because the hydroxyl radicals added most favorably at the *para*- and *ortho*- positions of the aromatic compound. This process occurred before the dechlorination event that forms hydroquinone and catechol which were further oxidized to benzoquinone. As displayed in Fig. 11c, the hydroxyl groups break the aromaticity and ring structure of the benzoquinone, generating simple acids, such as maleic, fumaric, and succinic acid. In the classical reaction scheme,[58] maleic, fumaric, and succinic acid decompose to form acrylic and oxalic acids. Acrylic acid appeared from the decarboxylation of maleic acid and is an intermediate in the pathway toward malonic and acetic acids. Acrylic acid was detected, and the subsequent oxidation products (malonic and acetic acids) were obtained. However, the produced oxalic and formic acids might come exclusively from maleic acid. Finally, the acetic and formic acids might be oxidized directly to form CO_2

and H_2O. Because the current efficiency was low during the practical application, it was unnecessary to mineralize 2,4-DCP to CO_2. Maintaining the degradation of 2,4-DCP to biodegradable aliphatic carboxylic acids was more valuable and attracting, due to these intermediates could subsequently be treated using more economical biologic treatment.

4. Conclusions

Preparation and investigation of a new Pd/graphene gas-diffusion cathode had been done to electro-catalytically dechlorinate and mineralize 2,4-DCP in water solutions. Palladium particles in the Pd/graphene catalyst averaging 5.4 nm in size had an amorphous structure with dispersing highly in the graphene. In the Pd/graphene gas-diffusion electrode system sequentially fed with hydrogen gas and air, the degree of 2,4-DCP dechlorination reached approximately 96.4% after 60 min The removal efficiency and the average removal efficiency of 2,4-DCP in the context of organic carbon (TOC) after 120 min reached approximately 100% and 90.5%, respectively. The Pd/graphene gas-diffusion cathode could catalyze reductive dechlorination of 2,4-DCP with H_2 feeding, and accelerated the two-electron reduction of O_2 to H_2O_2 in air. The degree of mineralization in cathodic chamber for organic compounds was higher than that in the anodic chamber, because of cathodic chamber where H_2O_2 and $HO\cdot$ generated in and cathode where the reductive dechlorination only performed in. The HPLC and IC data revealed the major intermediates of 2,4-DCP dechlorination the Pd/graphene gas-diffusion electrode system. The degradation efficiency of the chlorinated phenol was improved by combining reduction process with oxidation

process.

Acknowledgments

This work was supported by the Beijing Higher Education Young Elite Teacher Project (No. YETP0773), the National Natural Science Foundation of China (No. 51278053 and 21373032), and the Beijing Natural Science Foundation (No. 8122031).

References

1 J. Rivera-Utrilla, M. Sánchez-Polo, M. M. Abdel Daiem and R. Ocampo-Pérez, *Appl. Catal. B: Environ.*, 2012, **126**, 100-107.

2 L. J. Xu and J.L. Wang, *Appl. Catal. B: Environ.*, 2012, **123-124**, 117-126.

3 J. L. Rodríguez, M. A. Valenzuela, T. Poznyak, L. Lartundo and I. Chairez. *J. Hazard. Mater.*, 2013, **262**, 472-481.

4 H. Q. Jiang, Q. Y. Wang, S. Y. Zang, J. S. Li and Q. F. Wang, *J. Hazard. Mater.*, 2013, **261**, 44-54.

5 J. Liu, J. Y. Wu, C. L. Kang, F. Peng, H. F. Liu, T. Yang and L. Shi, H. L. Wang, *J. Hazard. Mater.*, 2013, **261**, 500-511.

6 B. Palanisamy, C. M. Babu, B. Sundaravel, S. Anandan and V. Murugesan, *J. Hazard. Mater.*, 2013, **252-253**, 233-242.

7 P. D. Leo, M. D. R. Pizzigallo, V. Ancona, F. D. Benedetto, E. Mesto, E. Schingaro and G. Ventruti, *J. Hazard. Mater.*, 2013, **244-245**, 303-310.

8 J. Xu, J. Tang, S. A. Baig, X. S. Lv and X. H. Xu, *J. Hazard. Mater.*, 2013, **244-245**, 628-636.

9 Q. Wen, T. Yang, S. Y. Wang, Y. Chen, L. J. Cong and Y. J. Qu, *J. Hazard. Mater.*, 2013,

244-245, 743-749.

10 H. Y. Zhao, Y. J. Wang, Y. B. Wang, T. C. Cao and G. H. Zhao, *Appl. Catal. B: Environ.*, 2012, **125**, 120-127.

11 X. P. Zhu and B. E. Logan, *J. Hazard. Mater.*, 2013, **252-253**, 198-203.

12 F. Matei, D. Ciuparu, C. Jiménez-Borja, F. Dorado, J. L. Valverde and S. Brosda, *Appl. Catal. B: Environ.*, 2012, **127**, 18-27.

13 S. J. Li, Y. L. Fang, C. D. Romanczuk, Z. H. Jin, T. L. Li and M. S. Wong, *Appl. Catal. B: Environ.*, 2012, **125**, 95-102.

14 R. Navon, S. Eldad, K. Mackenzie and F. D. Kopinke, *Appl. Catal. B: Environ.*, 2012, **119-120**, 241-247.

15 L. Calvo, A. F. Mohedano, J. A. Casas, M. A. Gilarranz and J. J. Rodríguez, *Ind. Eng. Chem. Res.*, 2005, **44**, 6661-6667.

16 G. Yuan and M. A. Keane, *Appl. Catal. B: Environ.*, 2004, **52**, 301-314.

17 L .Calvo, M. A. Gilarranz, J. A. Casas, A. F. Mohedano and J. J. Rodríguez, *Appl. Catal. B: Environ.*, 2008, **78**, 259-266.

18 M. Martin-Martinez, L. M. Gómez-Sainero, M. A. Alvarez-Montero, J. Bedia and J. J. Rodriguez, *Appl. Catal. B: Environ.*, 2013, **132-133**, 256-265.

19 H. Wang and J. L. Wang, *Appl. Catal. B: Environ.*, 2007, **77**, 58-65.

20 S. C. Shekar, J. K. Murthy, P. K. Kao and K. S. R. Rao, *Appl. Catal. A: Gen.*, 2004, **271**, 95-101.

21 G. Yuan and M. A. Keane, *J. Catal.*, 2004, **225**, 510-522.

22 P. P. Cellier, J. F. Spindler, M. Taillefer and H. Cristau, *Tetrahedron Lett.*, 2003, **44**, 7191-7195.

23 Q. W. Li, H. Yan, Y. Cheng, J. Zhang and Z. F. Liu, *J. Mater. Chem.*, 2002, **12**, 1179-1183.

24 X. G. Fu, Y. R. Liu, X. P. Cao, J. T. Jin, Q. Liu and J. Y. Zhang, *Appl. Catal. B: Environ.*, 2013, **130-131**, 143-151.

25 E. Antolini, *Appl. Catal. B: Environ.*, 2012, **123-124**, 52-68.

26 K. Gotoh, K. Kawabata, E. Fujii, K. Morishige, T. Kinumoto, Y. Miyazaki and H. Ishida, *Carbon*, 2009, **47**, 2112-2142.

27 K. X. Li, J. J. Xiong, T. Chen, L. S. Yan, Y. H. Dai, D. Y. Song, Y. Lv and Z. X. Zeng, *J. Hazard. Mater.*, 2013, **244-245**, 19-28.

28 J. Zhong, N. David, L. Wei, K. Carter and M. T. James, *Chem. Mater.*, 2010, **22**, 5695-5699.

29 X. F. Xia, W. Lei, Q. L. Hao, W. J. Wang and X. Wang, *Electrochim. Acta*, 2013, **99**, 253-261.

30 K. T. Chan, J. B. Neaton and M. L. Cohen, *Phys. Rev. B*, 2008, **77**, 235430-235441.

31 P. G. Ren, D. X. Yan, X. Ji, T. Chen and Z. M. Li, *Nanotechnol.*, 2011, **22**, 1-8.

32 A. Barras, M. R. Das, R. R. Devarapalli, M. V. Shelke, S. Cordier, S. Szunerits and R. Boukherroub, *Appl. Catal. B: Environ.*, 2013, **130-131**, 270-276.

33 K. S. Novoselov, A. K. Geim, S. V. Morozov, D. Jiang, Y. Zhang, S. V. Dubonos, I. V. Grigorieva and A. A. Firsov, *Science*, 2004, **306**, 666-669.

34 Z. S. Wu, W. C. Ren, L. B. Gao, B. L. Liu, C. B. Jiang and H. M. Cheng, *Carbon*, 2009, **47**, 493-499.

35 M. Zhou, Y. L. Wang, Y. M. Zhai, J. F. Zhai, W. Ren, F. Wang and S. J. Dong, *Chem. Eur. J.*, 2009, **15**, 6116-6120.

36 H. Wang, Z. Y. Bian, G. Lu, L. Pang, Z. P. Zeng and D. Z. Sun, *Appl. Catal. B: Environ.*, 2012, **125**, 449-456.

37 X. Z. Tang, Z. W. Cao, H. B. Zhang, J. Liu and Z. Z. Yu, *Chem. Commun.*, 2011, **47**, 3084-3086.

38 N. I. Kovtyukhova, P. J. Ollivier, B. R. Martin, T. E. Mallouk, S. A. Chizhik, E. V. Buzaneva and A. D. Gorchinskiy, *Chem. Mater.*, 1999, **11**, 771-778.

39 W. Hummers and R. Offeman, *J. Am. Chem. Soc.*, 1958, **80**, 1339-1339.

40 H. Wang and J. L. Wang, *Appl. Catal. B: Environ.*, 2009, **89**, 111-117.

41 H. K. He and C. Gao, *Sci. China Chem.*, 2011, **54**, 397-404.

42 A. R. Siamaki, A. R. S. Khder, V. Abdelsayed, M. S. El-Shall and B. F. Gupton, *J. Catal.*, 2011, **279**, 1-11.

43 H. L. Guo, X. F. Wang, Q. Y. Qian, F. B. Wang and X. H. Xia, *ACS Nano*, 2009, **3**, 2653-2659.

44 H. K. Jeong, Y. P. Lee, R. J. Lahaye, M. H. Park, K. H. An, I. J. Kim, C. W. Yang, C. Y. Park, R. S. Ruoff and Y. H. Lee, *J. Am. Chem. Soc.*, 2008, **130**, 1362-1366.

45 S. Park and R. S. Ruoff, *Nat. Nanotechnol.*, 2009, **4**, 217-224.

46 S. Bong, S. Uhm, Y. R. Kim, J. Lee and H. Kim, *Electrocatal.*, 2010, **1**, 139-143.

47 J. Prabhuram, T. S. Zhao, Z. K. Tang, R. Chen and Z. X. Liang, *J. Phys. Chem. B*, 2006, **110**, 5245-5252.

48 R. Kou, Y. Shao, D. Wang, M. H. Engelhard, J. H. Kwak, J. Wang, V. V. Viswanathan, C. Wang, Y. Lin, Y. Wang, I. A. Aksay and J. Liu, *Electrochem. Commun.*, 2009, **11**, 954-957.

49 P. Canizares, J. A. Domingues, M. A. Rodrigo, J. Villasenor and J. Rogdriguez, *Ind. Eng. Chem.*

Res., 1999, **38**, 3779-3785.

50 J. D. Rodgers, W. Jedral and N. J. Bunce, *Environ. Sci. Technol.*, 1999, **33**, 1453-1457.

51 J. F. Niu, D. Maharana, J. L. Xu, Z. Chai and Y. P. Bao, *J. Environ. Sci-China*, 2013, **25**, 1424-1430.

52 I. Sirés, J. A. Garrido, R. M. Rodríguez, E. Brillas, N. Oturan and M. A. Oturan, *Appl. Catal. B: Environ.*, 2007, **72**, 382-394.

53 U. D. Patel and S. Suresh, Sep. Purif. Technol., 2008, **61**, 115-122.

54 J. F. Niu, Y. P. Bao, Y. Li and Z. Chai, *Chemosphere*, 2013, **92**, 1571-77.

55 Z. R. Sun, X. F. Wei, Y. B. Han, S. Tong and X. Hu, *J. Hazard. Mater.*, 2013, **244-245**, 287-294.

56 Y. Yasman, V. Bulatov, I. Rabin, M. Binetti and I. Schechter, *Ultrason. Sonochem.*, 2006, **13**, 271-277.

57 Y. Wang, Z. Y. Shen, Y. Li and J. F. Niu, *Chemosphere*, 2010, **79**, 987-96.

58 A. Eftaxias, J. Font, A. Fortuny, J. Giralt, A. Fabregat and F. Stüber, *Appl. Catal. B: Environ.*, 2001, **33**, 175-190.